Computer-assisted Trajectory Planning for Percutaneous Needle Insertions

Authors and Affiliations

Alexander Seitel* MSc, Markus Engel* MSc

Division of Medical and Biological Informatics, German Cancer Research Center, Im Neuenheimer Feld 280, 69120 Heidelberg, Germany

Christof M. Sommer MD, Boris A. Radeleff MD

Department of Diagnostic Radiology, University of Heidelberg, Im Neuenheimer Feld 110, 69120 Heidelberg, Germany

Caroline Essert-Villard PhD, Claire Baegert PhD

Laboratoire des Sciences de l'Image, de l'Informatique et de la Télédétection, Pôle API, F67400 Illkirch, France

Markus Fangerau, Klaus H. Fritzsche PhD, Kwong Yung MSc, Hans-Peter Meinzer PhD, Lena Maier-Hein PhD

Division of Medical and Biological Informatics, German Cancer Research Center, Im Neuenheimer Feld 280, 69120 Heidelberg, Germany

**Authors contributed equally to this work*

Contact information

Alexander Seitel

German Cancer Research Center

Div. Medical and Biological Informatics (E130)

Im Neuenheimer Feld 280

69120 Heidelberg, Germany

Phone: +49 (0)6221 42 3550, Fax: +49 (0)6221 42 2345

e-mail: a.seitel@dkfz-heidelberg.de

Acknowledgement

The present study was conducted within the setting of Research Training Group 1126: "Intelligent Surgery – Development of New Computer-Based Methods for the Future Workplace in Surgery", funded by the German Research Foundation (DFG). The software for this project was developed within the open-source software framework MITK (http://www.mitk.org).

Short title

Trajectory Planning for Needle Insertions

Computer-assisted Trajectory Planning for Percutaneous Needle Insertions

Abstract

Purpose: Computed tomography (CT) guided minimally invasive interventions such as biopsies or ablation therapies often involve insertion of a needle-shaped instrument into the target organ (e.g. the liver). Today, these interventions still require manual planning of a suitable trajectory to the target (e.g. the tumor) based on the slice data provided by the imaging modality. However, taking into account critical structures and other parameters crucial to the success of the intervention - such as instrument shape and penetration angle - is challenging and requires a lot of experience.

Methods: To overcome these problems, we present a system for the automatic or semi-automatic planning of optimal trajectories to a target, based on 3D reconstructions of all relevant structures. The system determines possible insertion zones based on so-called *hard constraints* and rates the quality of these zones by so-called *soft constraints*. The concept of *pareto optimality* is utilized to allow for a weight-independent proposal of insertion trajectories. In order to demonstrate the benefits of our method, automatic trajectory planning was applied retrospectively to n=10 data sets from interventions in which complications occurred.

Results: The efficient (graphics processing unit-based) implementation of the constraints results in a mean overall planning time of about 9 seconds. The examined trajectories, originally chosen by the physician, have been rated as follows: in six cases, the insertion point was labeled invalid by the planning system. For two cases, the system would have proposed points with a better rating according to the *soft constraints*. For the remaining two cases the system would have indicated poor rating with respect to one of the *soft constraints*. The paths proposed by our system were rated feasible and qualitatively good by experienced interventional radiologists.

Conclusions: The proposed computer-assisted trajectory planning system is able to detect unsafe and propose safe insertion trajectories and may especially be helpful for interventional radiologist at the beginning or during their interventional training.

Key Words: interventional radiology, trajectory planning, radiofrequency ablation, image-guided therapy, computer-aided intervention

1 Introduction

Image-guided minimally-invasive interventions are gaining in importance in clinical routine today. Thermal ablation therapies, for example, are increasingly applied for treatment of focal malignant diseases. For 20% of all malignancies in the liver, surgical resection cannot be used for treatment, and radiofrequency ablation (RFA) emerged as a favored alternative [1]. This procedure requires insertion of a needle-shaped instrument into the cancerous tissue and therefore relies on precise planning of an appropriate insertion trajectory. Although protocols for manual trajectory planning are well established in clinical routine, the lack of three-dimensional (3D) presentation of the medical imaging data may lead to complications. Because the planning is mostly done on slice-based reformations of the 3D volume, the shape and length of the instrument can only be considered roughly and the penetration angle of the instrument is difficult to determine as well.

Several approaches to automatic trajectory planning have been presented in the context of neurosurgery. Although structures in the brain can be considered more rigid compared to abdominal organs, the process of planning a straight trajectory is similar for both body parts. The early work of Vaillant *et al.* [2] presents an algorithm that allows for automatically computing a rating of possible insertion points considering critical structures in the brain. The basic idea is to minimize a cost function over all possible paths that sums up individual, manually assigned voxel costs that take into account the critical structures. Brunenberg *et al* . [3] and Shamir *et al.* [4] [5] pointed out that this cumulative risk computation can be misleading and introduced the concept of risk volume, where each voxel is assigned a risk value dependent on the minimal distance to the surrounding critical structures. Thus, the manual assignment of cost values can be replaced by an efficient computation on distance maps. Shamir *et al.* also presented a quantitative clinical evaluation that showed improvements in procedure time and trajectory risk. Although these methods are quite efficient when considering the proximity of the trajectory to critical structures, it may be difficult to integrate other restrictions to the path which are of interest for interventions in the abdomen such as insertion angle or instrument shape. Navkar *et al.* [6] presented an approach based on projections of the critical structures on the head surface. They are thus able to detect trajectories which would hit or are too close to a critical structure and can also consider the length of the trajectories in their planning visualization. Nevertheless, they did not quantitatively evaluate their method on clinical data. Recently, Essert *et al.* [7] presented a method for automatic computation of electrodes trajectory for deep brain stimulation. Possible trajectories are determined by solving a set of geometric constraints. In a retrospective study on four patients, they could show the applicability of their method.

Automatic and semi-automatic approaches to trajectory planning in the abdomen are sparse. Most methods concentrate on calculation and simulation of the ablation zone and the resulting optimal probe placement with respect to the coverage of the tumor. Altrogge *et al.* [8] present a finite elements (FEM)-based approach for optimizing the needle placement taking into account the electric potential of the probe and the steady state of the heat distribution during RF ablation. The authors also present an integration of this optimization module into a workflow oriented software module (Weihusen *et al.* [9]). This includes tools for interactively planning the trajectory by defining the center of the necrosis zone and the position of the shaft of the needle in the CT slices. Butz *et al.* [10] also focus on optimizing the insertion trajectory with respect to the necrosis zone. Additionally, they use some basic three-dimensional visualization of the planned trajectory and the surrounding organs, allowing the physician to optimize the planning result. Zhai *et al.* [11] propose a framework for calculating a 3D visualization of the complete surgery scene including the trajectory and a 3D model of the necrosis zone. Starting from an interactively chosen insertion trajectory, the necrosis model is computed taking into account the microwave energy, the tissue temperature and the blood perfusion rate. Planning of the actual trajectory considering e.g. critical structures and an automatic rating of the chosen insertion point are not part of these methods.

Villard[12],[13],[14] and Baegert [15],[16],[17] propose a method based on a constraint concept for automatically computing insertion trajectories. An insertion trajectory consists of the given target point and an insertion point on the skin. So-called *hard constraints* are used to determine the insertion zones on the skin, which represent trajectories to the target that do not violate any restrictions to the path such as hitting a critical structure or exceeding the needle length. The quality of the trajectories that are allowed according to the *hard constraints* is then rated by so-called *soft constraints* that represent clinically relevant parameters such as the distance to critical structures. Several *soft constraints* can be combined using a weighted sum in order to obtain an overall rating of a given trajectory. Note that, as pointed out by Brunenberg *et al.* or Shamir *et al.*, weighted sum rating may be misleading. If a trajectory e.g. passes close to a critical structure but is also very short, the rating of the constraint considering the proximity to critical structures would be poor whereas the rating of the constraint considering the length would be good. Averaging these ratings could result in choosing this trajectory and a potential complication at the critical structure. Because all calculations are based on surface representations of the tumor, the liver, the skin and the critical structures, the proposed algorithms are still time consuming and require optimization. Using the concept of risk volume [5] could be an interesting alternative. Furthermore, a clinical evaluation showing the suitability of the proposed systems for interventions in the abdomen has not yet been conducted.

Recently, another planning approach has been proposed by Schumann *et al.* [18] where, as in Villard and Baegert, a set of constraints is used to determine suitable insertion trajectories. The authors use a method independent of the mesh representation of the critical structures by generating so-called *constraint maps* for each restriction by computing a cylindrical projection with the center at the target point. Each *constraint map* is rated by a constraint-specific rating function and merged to a weighted combination of all constraints. The maxima in this combined map correspond to the possible insertion trajectories. The authors report a total computation time of 6 seconds for determining optimal insertion trajectories on a standard computer. However, the weight factors of each constraint still must be set manually and an evaluation showing the clinical suitability of the proposed trajectory planning system has not yet been performed.

The main contribution of this work is two-fold. Firstly, we use the concept of *pareto optimality* which allows rating the trajectories weight-independently. Secondly, we evaluate an advanced version of the constraint concept for automatic trajectory planning retrospectively on a set of 10 clinical cases, in which complications occurred, to demonstrate the performance and clinical suitability of the proposed approach. The planning system aims to be helpful especially for unexperienced interventional radiologists and in difficult cases where e.g. the target is located close to a critical structure such as the heart.

The remaining part of this paper is organized as follows: First, we describe how the concept of *hard constraints* (section 2.1) and *soft constraints* (section 2.2) is realized. Then we concentrate on how to automatically select the best- suited trajectories using the concept of *pareto optimality* (section 2.3, 2.4). The design of the retrospective clinical study is presented in section 2.5. Finally, the results of the study are shown in section 3 and discussed in section 4.

2 Materials and Methods

We extend the work of Villard [14] and Baegert [15] to achieve a fast, robust, and extendable implementation for the automated trajectory planning. Although the main focus is on interventions in the liver, the system should be easy to adapt for usage in other body parts. Thus, a modular structure should allow integration of new constraints needed for different interventions. Also, the choice of the critical structures is not limited to a particular set but is entirely up to the interventional radiologist. In most cases of RFA liver interventions, bones, lungs, heart, stomach, gall bladder and big vessels are considered for planning. All components of the system have been developed within the Medical Imaging Interaction Toolkit (MITK) [19], a convenient platform for developing medical image processing applications, providing functionality similar to that of commercial image guided therapy systems. The computations for the planning result rely on mesh representations of the segmentations of skin, liver, tumor and critical structures which can be achieved with any segmentation tool. For this study, we used the semi-automatic, interactive approach presented by Maleike *et al.* [20].

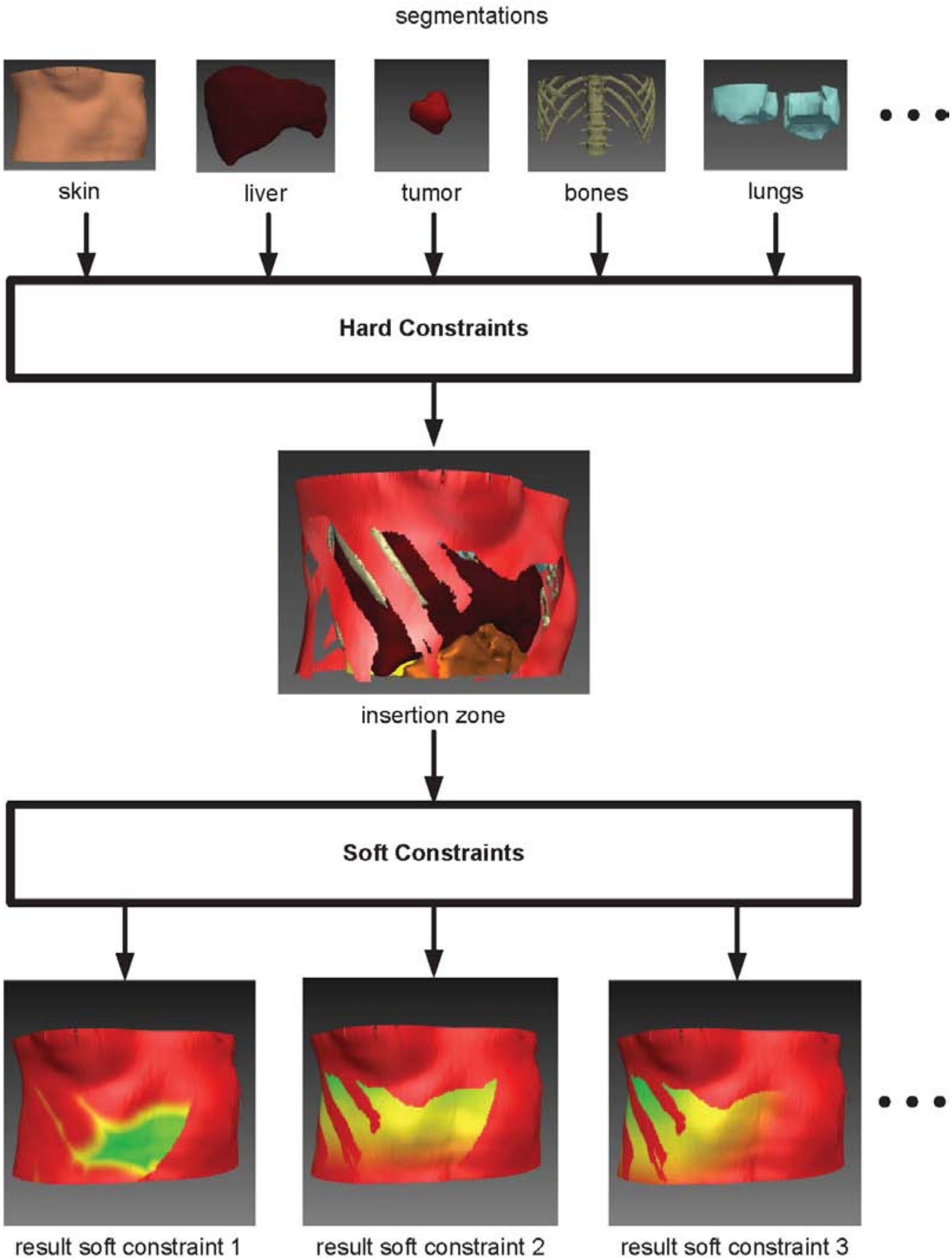

Figure 1. Constraint concept of the automatic trajectory planning. Surfaces of the skin, the liver, the tumor and other critical structures are created from corresponding segmentations. The insertion zone on the skin is determined using a combination of *hard constraints*. The points of the skin where insertion of the needle is not applicable are marked in red. A rating of those insertion zones is achieved by applying a combination of *soft constraints*.

The general optimization and extension of the constraint concept is described in section 2.1 and 2.2. The primary focus of this paper is on an additional, pareto-based planning interface for the physician (section 2.3) and a retrospective clinical study for quality assessment of the method (section 2.5).

2.1 Determination of insertion zones (*hard constraints*)

The points of the skin are progressively eliminated from the possible insertion zone by applying different *hard constraints* in a pipeline if the corresponding trajectory to the target does not satisfy the condition of the constraints (e.g. a maximum length of the trajectory) and thus would cause major complications during intervention. Each point in the resulting insertion zone (Figure 1) then defines a trajectory together with the predefined target point. Five different *hard constraints* have been implemented and used for this study and will be described in detail in the following paragraphs.

Occlusion Constraint

The *occlusion constraint* is used to determine those parts of the skin for which the corresponding insertion trajectory would not traverse any critical structure.

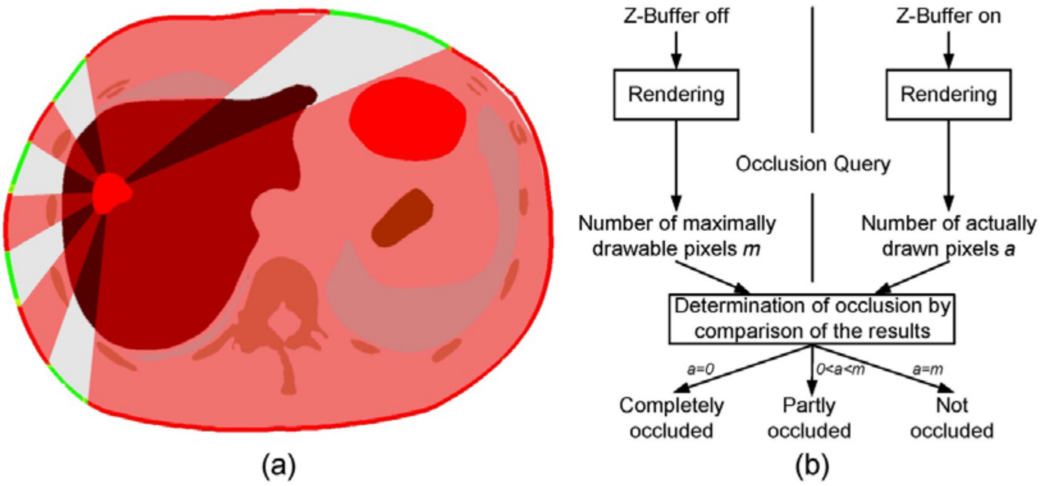

Figure 2. (a) Schematic illustration of the *occlusion constraint* and the determination of the insertion zone. All points of the skin that are visible from the target point are marked as possible insertion points. (b) Implementation of the *occlusion constraint* using fast occlusion queries. In a first rendering step with the Z-buffer turned off, the occlusion query returns the maximal number of drawable pixels for every triangle of the mesh of the skin (m). For the second rendering with the Z-buffer turned on, the occlusion query returns the number of actually visible pixels (a). The difference between these two values determines whether the triangle is completely visible (a = m), partly visible (0 < a < m) or not visible (a = 0).

The task of finding those points can be modeled as a line-of-sight problem, in which the virtual camera, which is used during the rendering[1], is placed at the target position. All points of the skin that are visible from this position - and thus not occluded by any critical structure - are marked as possible insertion points (Figure 2a). To allow for an efficient computation of these insertion zones, the so-called occlusion queries are used (Figure 2b). Every triangle of the mesh representing the skin is drawn (rendered) twice. In the first step with the Z-buffer[2] turned off, the maximal number m of drawable pixels is determined for each triangle. In the second run with the Z-buffer turned on, the number of actually visible pixels a of this triangle is returned. These numbers indicate whether the triangle is completely visible ($a = m$), partly occluded ($0 < a < m$) or not visible ($a = 0$).

This approach already uses the potential of modern graphics hardware, but still shows a performance leak as the central processing unit (CPU) and the graphics-processing unit (GPU) is not working parallel when a whole mesh is examined. The CPU has to wait for the GPU while the rendering of a triangle is in progress, and the GPU has to wait for the CPU, while the latter evaluates the result of the occlusion query. To overcome this problem, we introduced a buffer of occlusion queries, which will be extended as long as all triangles are rendered. The CPU in parallel reads the results of the completed queries from the buffer and processes it. This ensures a maximal utilization of resources.

Safety Margin around Target Constraint

The *safety margin around target constraint* ensures that a safety margin of at least 1 cm of healthy liver tissue is provided on that part of the trajectory located between the surface of the tumor and the liver capsule. This is needed to prevent bleeding and to allow cauterization and thus minimize the possible spreading of tumor cells. [21] Technically, this constraint marks parts of the liver surface as additional critical structures internally using the *occlusion constraint* as shown in Figure 3. Those critical structures are then considered by the “global“ *occlusion constraint*.

---

[1] **Rendering:** Process of generating an image of a scene (e.g. three-dimensional representation of different organs) from an underlying model (e.g. surface representation) of that scene

[2] **Z-Buffer:** Array of depth values of pixels generated during the rendering process. If two objects of the scene would be rendered into the same pixel, Z-buffering chooses the one closer to the camera.

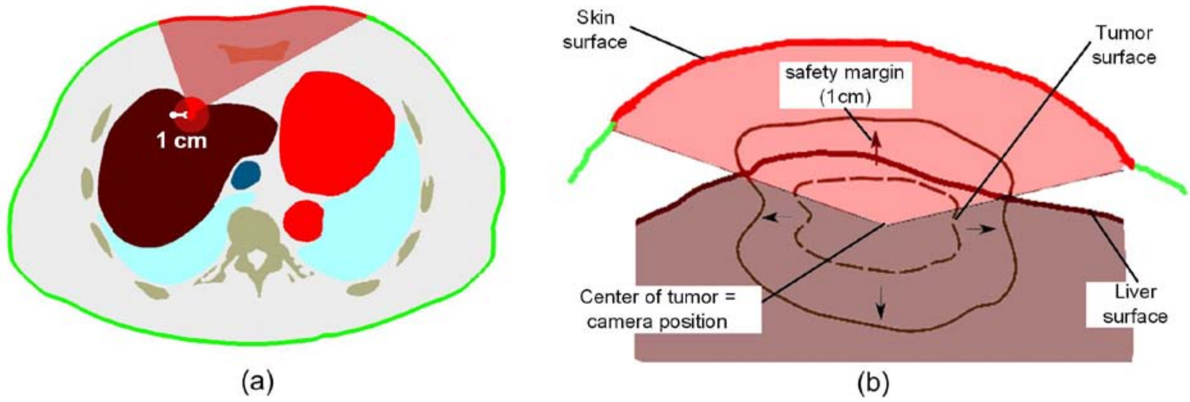

Figure 3. (a) Schematic illustration of the *safety margin around target constraint*, which ensures a safety margin of healthy liver tissue of 1cm on that part of the trajectory located between the surface of the tumor and the liver capsule. (b) Computation of additional critical structures for the *occlusion constraint*. First the tumor (dashed line) is dilated by the safety margin. Then the *occlusion constraint* is internally used to determine those parts of the liver that are visible from the center of the tumor. These represent the points which would result in a trajectory that does not cover the safety margin between the tumor surface and the liver capsule. Finally, these parts of the liver are defined as additional critical structures to be used by the *occlusion constraint*.

Tangency Constraint

The *tangency constraint* ensures that the angle in which the trajectory intersects the liver surface is bigger than 20° and therefore prevents the needle from slipping off the liver surface (Figure 4a). To allow for an efficient computation of the corresponding insertion zones, all triangles of the liver surface are determined for which the trajectory would show an insertion angle to the liver surface smaller than 20°. These triangles are then used as additional critical structures for the *occlusion constraint*.

Needle Length Constraint

The *needle length constraint* ensures that the trajectory is shorter than the needle to be inserted. All insertion points leading to a longer trajectory are eliminated from the insertion zone (Figure 4b).

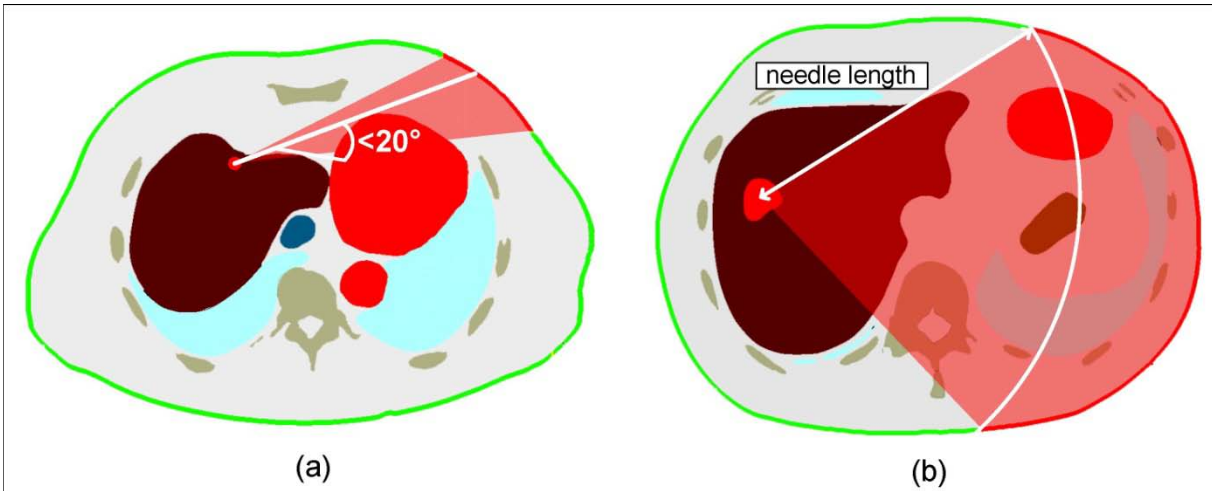

Figure 4. (a) Schematic illustration of the *tangency constraint,* which ensures that the angle in which the trajectory intersects the liver surface is bigger than 20°. (b) The *needle length constraint* excludes all insertion trajectories from the insertion zone that are longer than the needle.

RFA-Umbrella Constraint

Radiofrequency ablations are generally performed using a needle-shaped applicator. In order to enlarge the necrosis zone when treating large tumors, recent needle models offer the possibility to deploy a set of spikes that form a kind of umbrella. Common models currently used in clinical routine are the LeVeen® Electrode System and the Starburst™ Talon Device. Their deployed spikes can be represented by parts of a superquadric toroid which can be mathematically modeled using implicit functions that allow for fast and flexible computation of intersections with critical structures. In general, implicit functions are functions in which the dependent variable has not been given explicitly but as the solution of the equation $F(x, y, z) = 0$. They can be used for the mathematical description of a surface representation of an object [22]. Evaluating the so-called inside-out function $F(x, y, z)$ allows to decide whether the corresponding point (x, y, z) lies inside ($F(x, y, z) < 0$), outside ($F(x, y, z) > 0$) or on the surface ($F(x, y, z) = 0$).

The *RFA-umbrella constraint* ensures that this additional umbrella does not hit any critical structure (Figure 5). The inside-out function is defined by a superquadric toroid $T(x, y, z) = \left(r_c - \sqrt{x^2 + y^2}\right)^2 + z^2 - {r_a}^2$, where r_c is the radius from the center of the torus to the center of the torus tube and r_a is the radius of the torus cut by the six planes that form a box with the extents a, b, and c (Figure 5c). For every insertion trajectory and the corresponding orientation of the umbrella, the resulting implicit function is evaluated for every point of the surface of the critical structures. If one of the resulting values is smaller than 0, the corresponding insertion point on the skin is eliminated from the insertion zone. Note that if no surface point is located inside the umbrella model, the umbrella is located completely outside or inside of a critical structure. The inside case, which would cause complications that could not be detected by this constraint, is not possible because the target would also have to lie inside the critical structure.

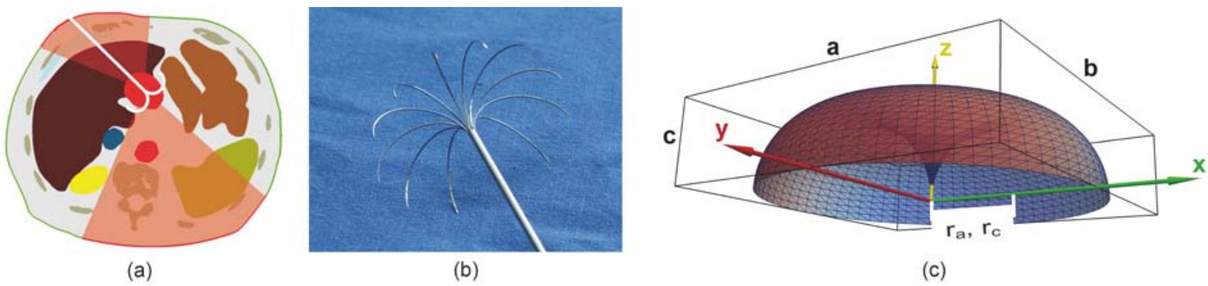

Figure 5. (a) Schematic illustration of the *RFA-umbrella constraint* that ensures the umbrella- shaped electrode of the RFA needle does not hit any critical structures. (b) Prong umbrella of LeVeen® Electrode System. (c) Surface representation using implicit function.

2.2 Rating of insertion zones (*soft constraints*)

The previously determined insertion zones are rated by three different *soft constraints* defined by a corresponding cost function, each representing one clinically relevant parameter (Figure 6). All *soft constraints* are normalized to allow for a weighted combination as reported by Villard/Baegert [17]. The rating value of the *soft constraints* is between 0 and 1, where 0 refers to an invalid trajectory and 1 refers to a trajectory that is considered relatively safe.

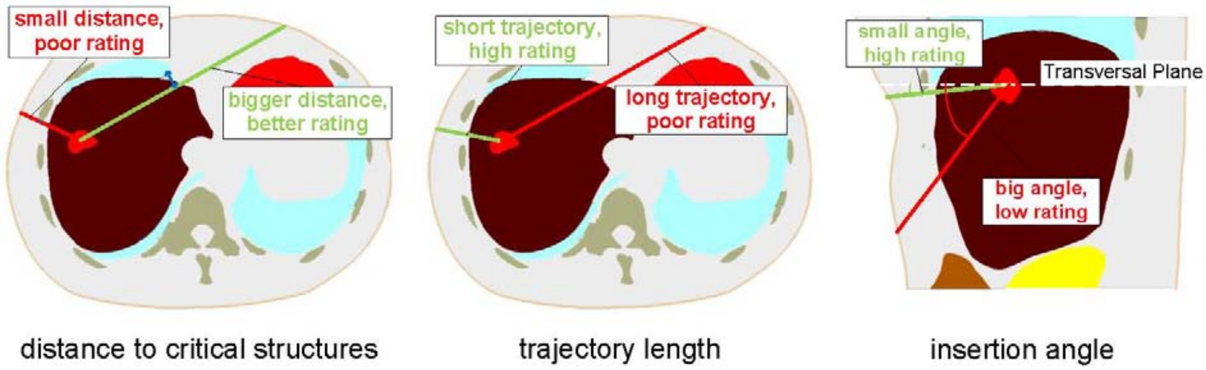

Figure 6. Rating of the insertion zones by the *soft constraints*: The *distance to critical structures constraint* rates the possible insertion trajectories according to their distance to critical structures. The length of the trajectory is considered by the *trajectory length constraint.* The insertion angle constraint prefers trajectories that have a small angle to the axial slice the target lies in.

Distance to critical structures constraint

The *distance to critical structures constraint* (DTCS) c_1 rates the possible insertion trajectory tr according to its distance $d(tr)$ to critical structures, which is defined as the shortest distance between the insertion trajectory and any mesh point of the critical structures. The bigger the distance is, the better the trajectory is rated. To reduce computation time, the mesh points of all critical structures are initially stored in so-called KD-trees [23] which represent a data structure that allows for high performance navigation in a large set of points. The rating is computed as follows:

$$r_{c_1}(tr) = \frac{d(tr) - d_{min}}{d_{max} - d_{min}}$$

where d_{min} and d_{max} are the minimal and maximal distance to critical structures, respectively.

Trajectory length constraint

The trajectory length $l(tr)$ is considered by the *trajectory length constraint* (TL) c_2. The shorter the trajectory, the better the corresponding insertion point is rated with the rating being proportional to the trajectory length. The rating is computed as follows:

$$r_{c_2}(tr) = 1 - \frac{l(tr) - l_{min}}{l_{max} - l_{min}}$$

where l_{min} and l_{max} are the minimal and maximal trajectory length, respectively.

Insertion angle constraint

Physicians often tend to insert the needle in the axial slice as acquired by the CT (in-plane). Therefore, the *insertion angle constraint* (IA) c_3 rates those trajectories better that are closer to the axial plane the target is in. It thus reduces the number of degrees of freedom which have to be considered when transferring the plan to the patient. Furthermore, the trajectory can be confirmed more easily in a control CT scan. The rating is calculated from the insertion angle $\alpha(tr)$ according to an exponential scoring function, which was determined empirically:

$$r_{c_3}(tr) = \begin{cases} e^{-\frac{\alpha(tr)^2}{20^{\circ 2}}}; \ \alpha(tr) \leq 40^\circ \\ \\ 0 \ \ ; \ \alpha(tr) > 40^\circ \end{cases}$$

2.3 Semi-automatic selection of a trajectory

Given the insertion zones, there are now many candidates for an insertion point of the trajectory. To decide on the final path, the control is returned to the radiologist who chooses the one he personally rates best. To support him with this decision, we developed two alternatives to assist planning of the final insertion trajectory. Firstly, as proposed by Baegert *et al.* [15], a proposal for suitable insertion trajectories can be achieved by adapting the weights of the *soft constraints* (section 2.3.1). Secondly, the principle of *pareto optimality* can be used for a weight-independent proposal of appropriate insertion trajectories (section 2.3.2).

2.3.1 Weight-based trajectory planning

To achieve a rating of the insertion zones, the normalized result $r_{c_i}(tr)$ of each soft constraint is considered in a weighted sum.

$$R(tr) = \sum_{i=1}^{n} w_i r_{c_i}(tr \quad)$$

The individual weighting factors w_i are manually selected with $\sum_{i=1}^{n} w_i = 1$. The resulting rating R is visualized in the insertion zone using a color gradient ranging from green ("good rating", big R) to red ("poor rating", small R). An update of the weights leads to a change of the color gradient (Figure 7). For planning the final insertion trajectory, the insertion point can simply be marked by clicking on the desired location on the skin. As an extension of the work of Villard and Baegert, a set of better points (at least better in one parameter and not worse in another one) can be shown (Figure 8 and 9b).

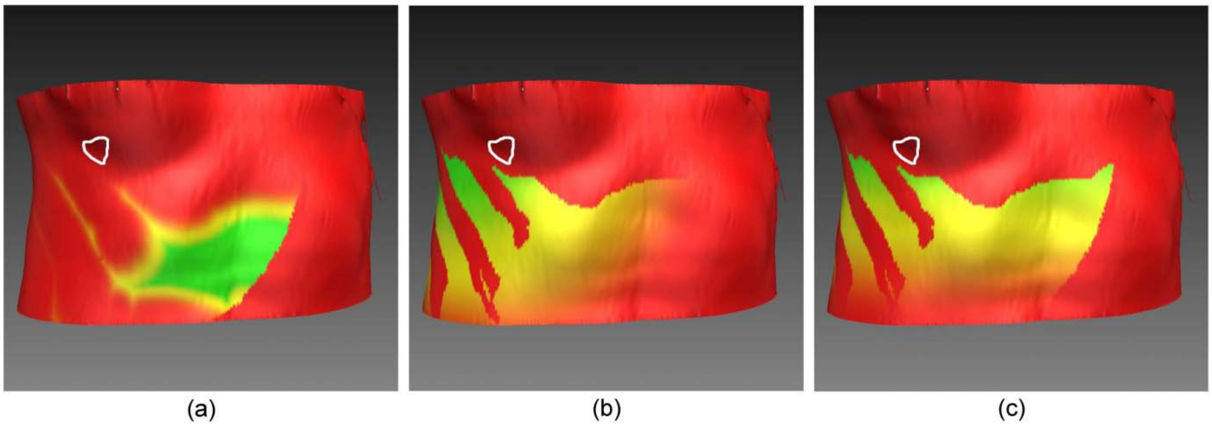

Figure 7. Color coded insertion zones for differently weighted combinations of the *soft constraints* based on the same combination of *hard constraints*. 100% means that the weight was 1 for the examined constraint and 0 for the other constraints. The contour of the tumor is drawn in white. (a) 100% distance to critical structures. (b) 100% insertion depth. (c) 100% in-plane.

2.3.2 Pareto-based trajectory planning

To provide an automatic way of planning a trajectory, the principle of *pareto optimality* [24] is used to determine suitable insertion trajectories without the need of weights (Figure 8). A point in a set of points is called *pareto-optimal* if there is no other point in this set that scores better in one parameter without scoring worse in another one. The set of all *pareto-optimal* points is called *pareto frontier*. In our case, the parameter space is spanned by the individual *soft constraints*. Applying the pareto-based optimization, the system can either show all *pareto-optimal* points as a proposal for trajectories or the intersection between this *pareto frontier* and the set of better points (cf. section 2.3.1) calculated from a chosen insertion point (Figures 8,9). This allows providing the physician with an automatically generated proposal and directs his attention towards those regions of the insertion zone, which are best suited for an insertion.

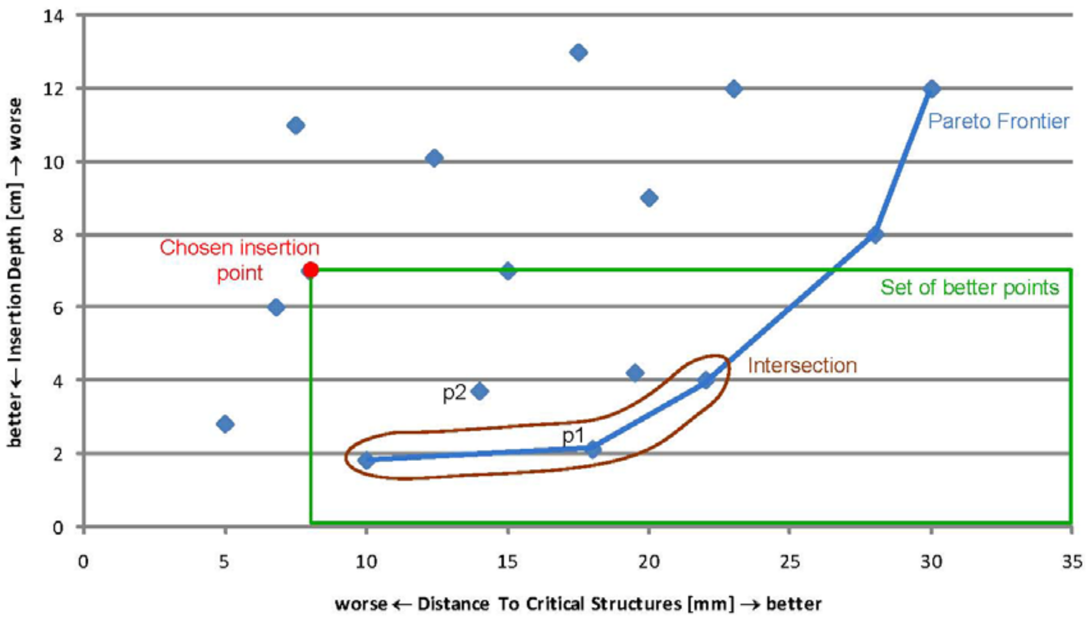

Figure 8. Illustration of the concept of *pareto optimality* and trajectory selection explained for a two-dimensional parameter space with the parameters insertion depth and distance to critical structures. A point (e.g. p1) is called *pareto-optimal* if there is no other point that scores better in one parameter without scoring worse in another. Point p2 is not *pareto-optimal* because p1 scores better in both parameters. The line at the edge of the point cloud is called *pareto frontier* and includes all *pareto-optimal* points. The rectangle marks all points that are in at least one parameter better suited than the chosen insertion point. They form the so-called set of better points for a given insertion point. The intersection between the *pareto frontier* and the set of better points contains all points that are *pareto-optimal* and in all parameters better suited than the chosen insertion point.

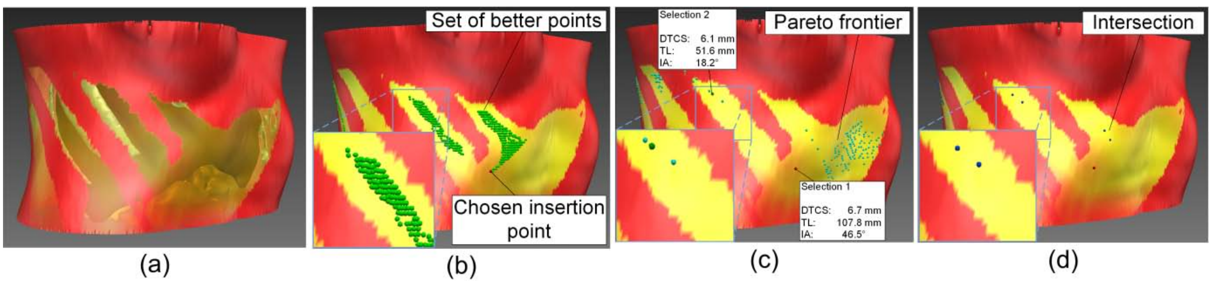

Figure 9. Different types of trajectory selection assistance. (a) Transparent insertion zone (b) Set of better points (green) which score in at least one parameter better than the chosen insertion point (red). (c) *Pareto frontier* (blue) showing all *pareto-optimal* points, i.e. the set of points for which there is no other point, which scores better in one parameter without scoring worse in another one. Two selections are marked and the quantitative measures of the *soft constraints* distance to critical structures (DTCS), trajectory length (TL) and insertion angle (IA) are provided. (d) Insertion points lying both on the *pareto frontier* and in the set of better points (dark blue).

2.4 Slice-based correction

The slice-based planning offers the physician the possibility to plan or refine a trajectory on reconstructed slices of the CT dataset (axial, sagittal, and coronal) or in an interactive three-dimensional view. A point-and-click interface allows for easy interaction with the trajectory. Additionally, there is a possibility to step through the planned trajectory and to reconstruct slices of the data set, in which the trajectory is completely visible. All relevant structures can be visualized in the two-dimensional slices and the three-dimensional view (Figure 10).

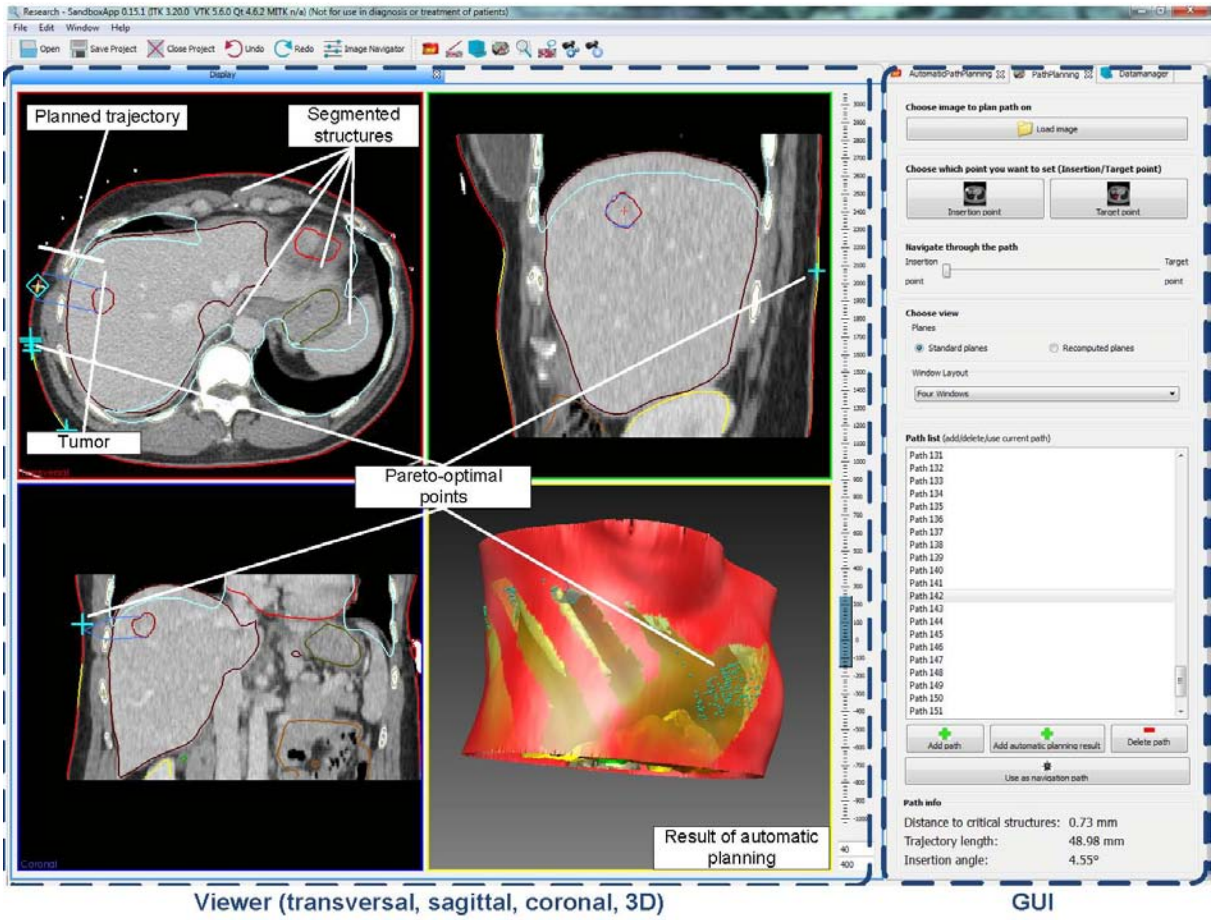

Figure 10. Trajectory planning interface realized within the Medical Imaging Interaction Toolkit (MITK [19]). On the left side, the user can view the medical imaging data in multiple planar reconstructions (transversal, sagittal, coronar) and also has interactive access to a 3D viewer which presents e.g. 3D surface data. On the right, the graphical user interface (GUI) for the trajectory planning provides tools for both automatic planning and manual trajectory refinement.

2.5 Evaluation

The evaluation of the proposed system for automatic trajectory planning was performed in a retrospective study on n=10 clinical datasets which showed complications during the intervention (e.g. pneumothorax, Table 1). The interventions were performed by different interventional radiologists. For each intervention, a pre-interventional planning CT scan and multiple intra-interventional control CT scans were acquired. To reduce the radiation exposure to the patient, the control scan did only cover that region of the image showing the needle. In order to facilitate the extraction of the chosen insertion point, the control scan was registered to the planning scan using a point-based registration method [25]. Due to the retrospective nature of the study, the planning and control scan were not always acquired in the same state of respiration. This affects the position and size of the lungs in particular which have to be considered as critical structures. To compensate for this and for breathing motion in general, we dilated the lung meshes by 12 mm, which represents the mean lung motion in cranial-caudal direction (Seppenwoolde *et al.* [26]). Skin, liver, tumor, and critical structures were segmented manually using the interactive segmentation framework of MITK [20].

Case	**Intervention**	**Complication**	**Needle type**
1	Liver RFA	Pneumothorax	Single needle
2	Liver RFA	Pneumothorax	Single needle
3	Liver RFA	Pneumothorax	Starburst umbrella needle (∅3cm)
4	Liver RFA	Pneumothorax	LeVeen umbrella needle (∅2cm)
5	Liver RFA	Pneumothorax	LeVeen umbrella needle (∅2cm)
6	Liver RFA	Pericardal effusion	Starburst umbrella needle (∅3cm)
7	Liver RFA	Hematothorax	LeVeen umbrella needle (∅2cm)
8	Liver RFA	Pneumothorax	Starburst umbrella needle (∅3cm)
9	Drainage	Pneumothorax	Single needle
10	Drainage	Pneumothorax	Single needle

Table 1. Data sets used for the retrospective evaluation. The type of intervention, the type of complication and the type of the needle used are shown. For the cases 9 and 10, the targets did not lie inside the liver. Therefore, the liver specific constraints *safety margin around target* and *tangency* were not applied.

The automatic planning was performed on all 10 datasets using a desktop computer (Intel® Core™i7, 2.93 GHz, 3.23 GB RAM, GeForce 8800GT, Windows XP, 32 bit).

For the technical evaluation, the runtime of each constraint and the remaining insertion zone after application of the *hard constraints* were determined.

In the clinical evaluation, the result of the automated planning was retrospectively compared to the clinically chosen trajectory to investigate, whether the *hard constraints* would have prohibited the planned trajectory or if it would have been rated poorly by (one of) the *soft constraints*.

To assess the validity of the tractories proposed by our system, we asked two interventional radiologists with experience in punctures and RFA (R1: more than 2500 punctures and more than 300 RFAs, R2: more than 200 punctures and more than 50 RFAs) to use our software to select one point on the *pareto frontier* as potential insertion point for each of the ten cases of our retrospective data set. The experts were then asked to qualitatively compare the corresponding path with the actually chosen path by answering the following questions:

- Is the path proposed by the system a good proposal given the anatomy of the patient?
- Was the chosen insertion point a good choice?
- Which path would you prefer?

3 Results

Figure 11 illustrates the trajectory planning procedure performed for one of the ten patients for each step of the workflow and the resulting surface with transparent green insertion zone. Table 2 shows the mean execution times of the *hard constraints* and the *soft constraints*. Note that the execution of the *hard constraints* in the pipeline progressively eliminates points from the insertion zone and thus reduces the execution time for the constraints applied last in the pipeline. The execution time of the *hard constraints* ranged from 0.02 ±0.00 s for the *needle length constraint* to 4.13 ± 0.55 s for the *RFA-umbrella constraint*. The *soft constraints* took 0.02 ± 0.00 s (*insertion depth*), 0.01 ± 0.00 s (*insertion angle*) and 3.18 ± 3.13s (*distance to critical structures*), respectively. The umbrella constraint could profit most from the execution in the constraints pipeline and could be executed about 38 s faster. The mean overall execution time of the entire automatic trajectory planning was 9.23 ± 5.15 s. Due to an improved GPU based implementation of the *occlusion constraint* its execution time could be decreased from 24.39 ± 3.10 s for the approach as presented by Villard and Baegert to 2.48 ± 0.20 s using similarly sized meshes, which is an improvement of 90%.

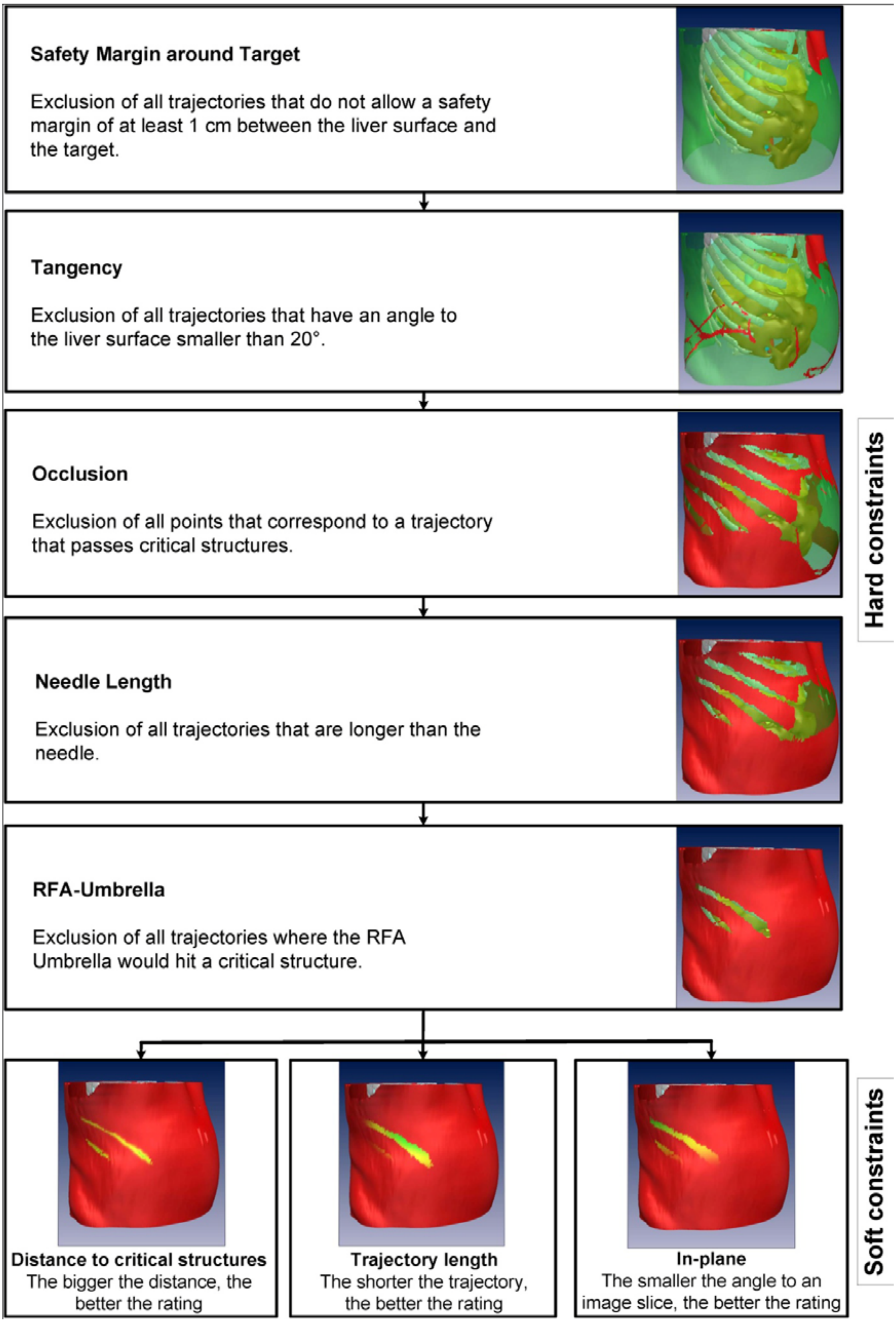

Figure 11. Trajectory planning workflow and resulting surfaces. For the *hard constraints*, the insertion zone is shown transparently green. The result of the *soft constraints* is visualized with a color gradient ranging from red (poor rating) to green (good rating).

	Constraint	Time (s)
	Safety margin around target (n=8)	1.27 ± 0.18
	Tangency (n=8)	0.04 ± 0.01
HC	Occlusion (n=10)	2.48 ± 0.20
	Needle Length (n=10)	0.02 ± 0.00
	Umbrella (n=6)	4.13 ± 5.29
	Distance to Critical Structures (n=10)	3.18 ± 3.13
SC	Insertion Depth (n=10)	0.02 ± 0.00
	Insertion angle (n=10)	0.01 ± 0.00

Table 2. Mean execution time in s for each *hard constraint* (HC) and *soft constraint* (SC) averaged over the specified number of datasets applicable for that constraint.

Considering the remaining area for possible insertion points on the skin, the *occlusion constraint* is the most restrictive constraint, leaving only 18% of the patient's skin as insertion area. The *tangency constraint* in contrast leaves 93% for possible insertion (*safety margin around target*: 88%, *needle length*: 43%, *umbrella*: 5%).

Case	**Complication**	**Expected result (organ)**	**Trajectory excluded?**
1	Pneumothorax	Occlusion (lung)	No
2	Pneumothorax	Occlusion (lung)	No
3	Pneumothorax	Occlusion (lung)	Yes
4	Pneumothorax	Occlusion (lung)	Yes
5	Pneumothorax	Occlusion (lung)	Yes
6	Pericardial effusion	Umbrella (heart)	Yes
7	Hematothorax	Occlusion (lung)	Yes
8	Pneumothorax	Safety margin around target (liver)	Yes
9	Pneumothorax	Occlusion (lung)	No
10	Pneumothorax	Occlusion (lung)	No

Table 3. Performance of the *hard constraints.* For all 10 cases with complications, the *hard constraint* expected to exclude the chosen trajectory is given together with the actual exclusion result

As **Table 3** shows, the initially chosen insertion point was declared invalid by the planning system for six cases (3-8). For these cases, the correct *hard constraint* excluded the chosen trajectory. In case 3, for example, a pneumothorax occurred and the *occlusion constraint* declared the insertion point illegal with the lung being the restrictive critical structure. For the cases 1, 2, 9 and 10 the *hard constraints* did not exclude the chosen insertion points even though a pneumothorax occurred in those cases. The reader may be reminded that the respiratory motion causes an additional uncertainty for the planning in the position of the lungs. Additionally, due to the retrospective nature of this study, the organ positions in the planning and the control CT may differ. **Table 4** shows that in two of the four cases in which the chosen insertion point was valid, better points could be found for which the rating of one or more *soft constraints* could be improved without worsening the remaining *soft constraints*. For the two cases, where the automatic proposal could not find better points, the physicians tended to choose a short insertion trajectory close to critical structures and almost in-plane.

Case	**Improvement possible?**	**Better points (% of insertion zone)**			**Insertion zone (cm^2)**
		DC	TL	IA	
1	No	89.0	0.03	1.9	293
2	No	62.3	0	32.9	220
9	Yes	12.6	52.0	5.2	81
10	Yes	33.1	9.3	50.1	91

Table 4. Quality of the chosen insertion point for the four data sets where the chosen insertion point was declared valid by the *hard constraints*. The table shows if an improvement of the rating of one or more *soft constraints* was possible without worsening the rating of the remaining constraints and how many points (in percentage of the total number of points in the insertion zone) showed a better scoring with respect to every single *soft constraints* (DC = distance to critical structures, TL = trajectory length, IA = insertion angle). The size of the insertion zone given in cm^2.

Figure 12 shows the chosen insertion point compared to all other points of the insertion zone regarding the scores of each *soft constraint* for the four cases where the chosen trajectories were not excluded by the *hard constraints.* In two of the four cases (1, 2), the physician chose trajectories which were *pareto-optimal*. In both cases the path was chosen with a short *trajectory length*, because these trajectories were technically easier to transfer to the patient. In contrast, many insertion points with a bigger *distance to critical structures* could be found while only slightly increasing the *insertion depth* or the *insertion angle*. In case 9 the trajectory was almost chosen *in-plane* with a sufficiently big *distance to critical structures* while the resulting length of the trajectory was rather long. Furthermore, the *insertion depth* could have been decreased without increasing the *insertion angle* or decreasing the *distance to critical structures*, i.e., the chosen insertion point was not *pareto-optimal*. In case 10, the trajectory length was considerably short, while the *distance to critical structures* was very small and the angle to the transversal plane relatively big. The insertion point was almost *pareto-optimal*, but the system identified several points with a smaller insertion angle which decreases the uncertainties of an angulated needle insertion.

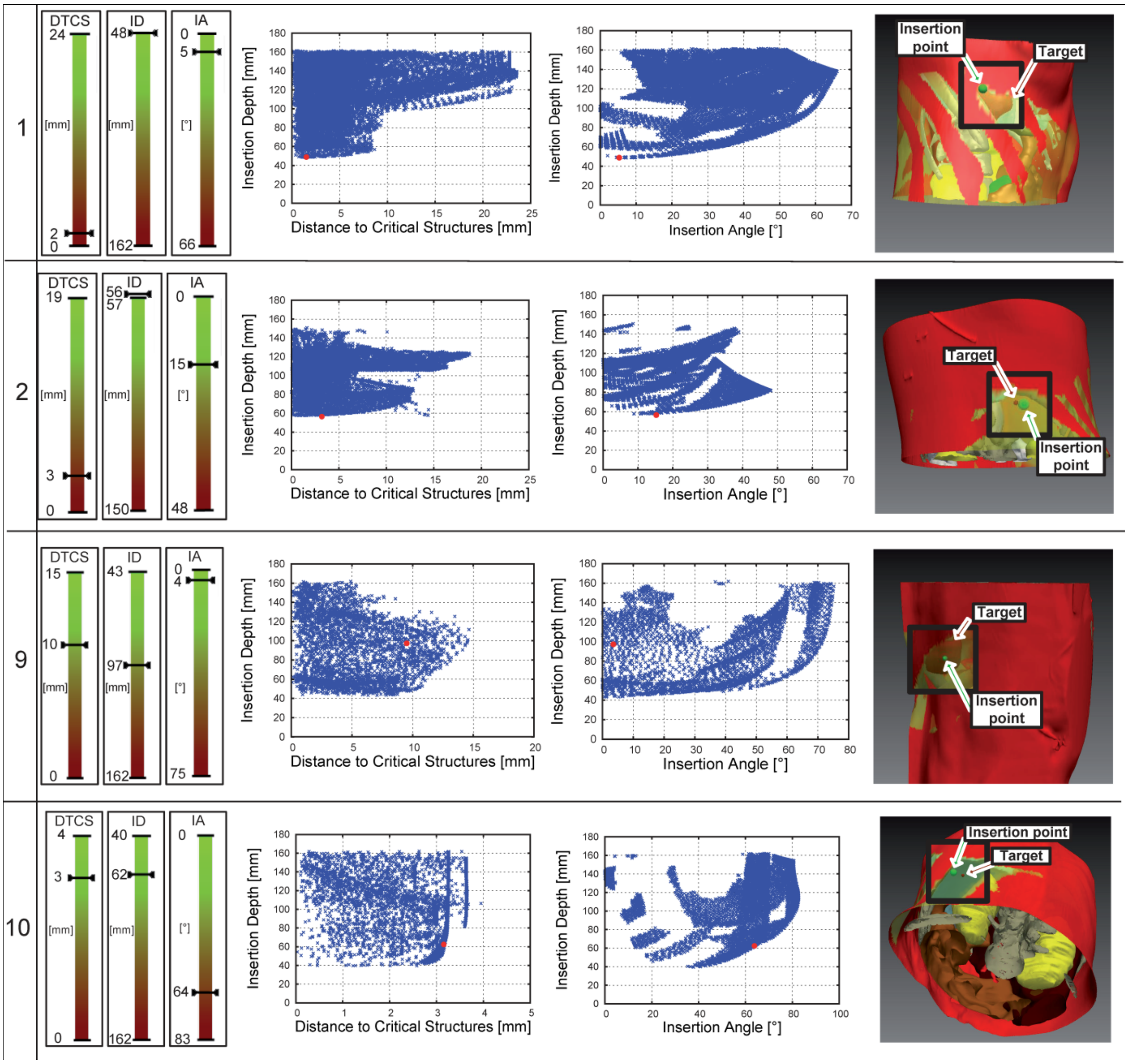

Figure 12. Results of the *soft constraints* for the four cases where the chosen insertion point was not excluded by the *hard constraints*.(a) Score of the chosen insertion point visualized for each *soft constraint* in a bar graph ranging from the worst to the best score. (b)+(c) Plots of the scores of all points in the insertion zone and the chosen insertion point each shown for two of the *soft constraints*. (d) Surface representation of the whole scene which shows the color-coded skin, critical structures, and the target and insertion point chosen by the physician.

Figure 13 and Table 5 summarize the results of the quality assessment of the proposed trajectories.

R1 rated the trajectory he selected with the planning system better than the original path in all cases and needed 3 minutes on average for the selection. However, for the cases 5 and 6 a suitable trajectory could only be found when not using the *umbrella constraint* because in this cases the radiologist would not have fully deployed the spikes of the umbrella to cover the tumor, like it is assumed by the constraint. R2 could find better trajectories in all cases but case 6 and also needed 3 minutes on average for the trajectory selection. For the cases 4, 5, 6 and 8 the *umbrella constraint* was not used to select a trajectory. In some cases (4, 6, 9) several proposed trajectories were rated poorly because they would hit the portal vein which was not included as a critical structure, because no contrast enhanced CT scan was available. Our radiologists, however, would have used such an additional scan for planning a safe trajectory. Furthermore two trajectories (case 8 and 10) were rated technically good but difficult to perform. According to R1, the use of a navigation system such as the one of Maier-Hein *et al.* [27] would be beneficial in these cases. Quantitatively, the trajectories chosen by the radiologists were more distant to critical structures but longer compared to the originally chosen insertion point.

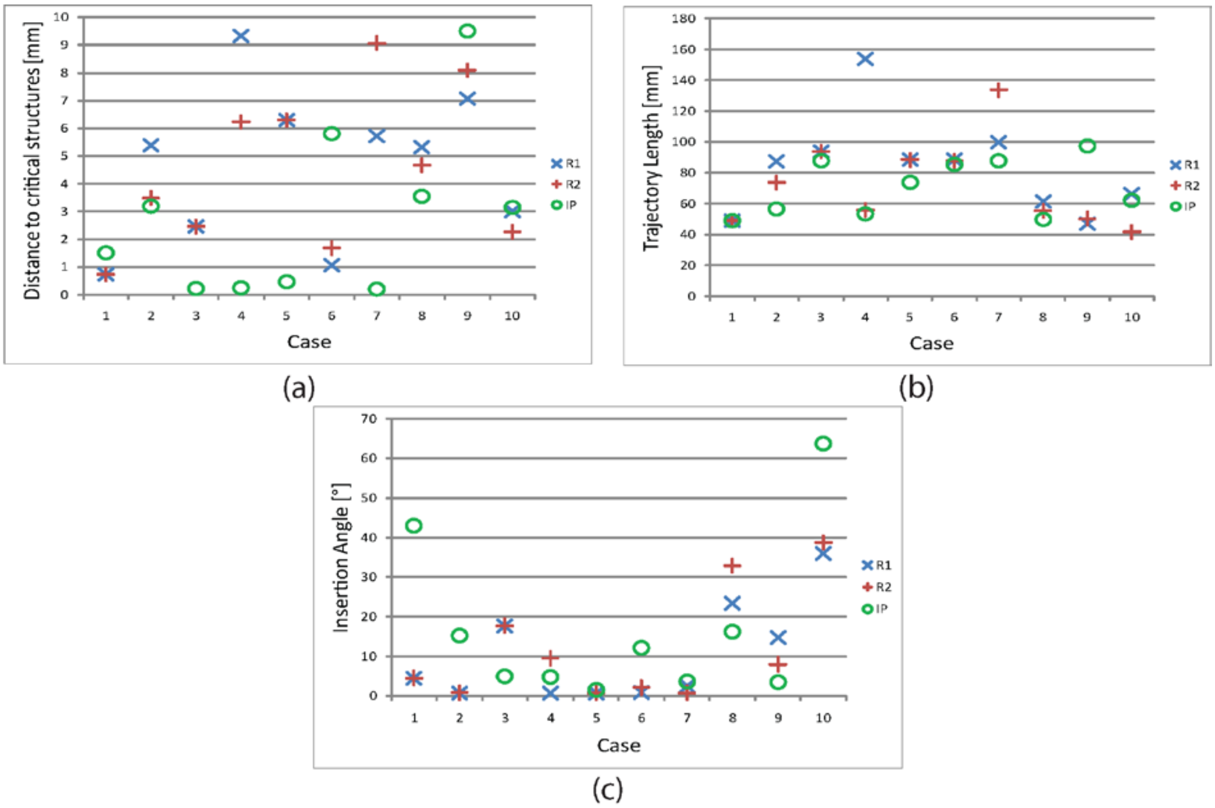

Figure 13. Quality assessment of the *pareto-optimal* points proposed by the planning system. Two interventional radiologists (R1, R2) each chose the subjectively best point from the *pareto frontier*. The corresponding quantitative measures distance to critical structures (a), trajectory length (b), and insertion angle (c) are shown for the selected points and the originally chosen insertion point (IP). Note that the radiologists could only find suitable points when not using the umbrella constraint in the cases 5, 6 (R1) and 4, 5, 6, 8 (R2).

Case	**1**		**2**		**3**		**4**		**5**		**6**		**7**		**8**		**9**		**10**	
	R1	R2	R1	R2	R1	R2	R1	R2	R1	R2	R1	R2	R1	R2	R1	R2	R1	R2	R1	R2
better?	+	+	+	+	+	+	+	+	+	+	+	-	+	+	+	+	+	+	+	+
time (min)	7	7	1	3	2	3	1	2	8	2	2	2	1	2	1	2	2	2	1	1
# points	155		16		5		56		40		19		74		97		75		38	

Table 5. Selection of the insertion point from the *pareto frontier* and comparison with the original insertion point. The rows show whether the point that was selected by the interventional radiologist (R1 or R2) was better than the original point (better?) according to the radiologist himself. Time represents the duration of the manual part of the planning process based on the *pareto frontier*. # points ist the number of points on the *pareto frontier*.

4 Discussion

To our knowledge, we are the first to present a weight-independent approach for automatic trajectory planning in the abdomen. We could show in a retrospective study that our system is capable of preventing the user from choosing trajectories which are likely to lead to complications during an intervention. According to radiological experts, the trajectories proposed by the planning system are useful and valid for intervention. Only for one of the ten cases, the proposed path was rated poorly. Computation of a trajectory proposal based on an efficient implementation of the applied hard and *soft constraints* took about 9 seconds on average. The selection of an insertion path based on the proposal by the radiologist took 3 minutes on average.

The presented approach was designed to be extendable and can easily be adapted for other body parts in a straightforward manner. As there are currently no constraints as for needle and patient position, constraints ensuring that e.g. the inserted needle still fits in the gantry of the CT scanner or the patient is always supposed to be in supine position can be added to the automatic path planning workflow in a straightforward manner. In fact, integration of such constraints was also proposed by the radiologists that used the system. Similar approaches from Villard and Baegert [17] or Schumann *et al.*[18] also concentrate on the computation of suitable insertion trajectories, but still depend on an appropriate weighting of the different constraints to achieve the desired planning result. Utilizing a pareto-based optimization, our approach is able to propose insertion trajectories without needing weights. Furthermore, the suitability of the approaches of Baegert *et al.* and Schumann *et al.* to support radiofrequency ablations or biopsies have not yet been evaluated in a clinical study.

As the state in the breathing cycle crucially affects both the poses and the dimensions of critical structures such as the lungs, it also has a high influence on the result of the planning. This could explain why only in six out of ten cases the chosen trajectories have been excluded by the system and that for two of the remaining cases no better trajectories could be found. We aimed to compensate for this by dilating the lung by the average lung movement. Incorporating a respiratory model for the lungs and the organs in the abdomen could possibly further improve the planning result. Furthermore, the respiratory states for intervention planning and needle insertion should be identical in future applications of the planning system. In this work we could not consider this issue due to the retrospective nature of the study. Nevertheless, the majority of the points of the insertion zone had a better rating by the *distance to critical structures constraint* compared to the chosen insertion point.

The use of surface meshes for the computation of the insertion zones leads to a dependency on the quality and the resolution of the mesh. The *tangency constraint* requires smooth meshes, as the angle to the liver surface is computed using the surface normals. Especially the *distance to critical structures constraint* and the newly proposed *RFA-umbrella constraint* strongly depend on the resolution of the meshes, because all mesh points of the critical structures are considered for computation of the planning result. Thus, the resolution of the mesh has to be carefully chosen to find a balance between runtime and planning accuracy. The *occlusion constraint*, directly using graphics rendering for computation, is also limited by the resolution of the used screen. We are currently working on a so-called off-screen rendering, which allows performing the rendering on arbitrary sized, virtual screens.

As a mesh representation of every critical structure is required for the trajectory planning, the fast segmentation of the liver, the critical structures, the skin and the target in the CT image, preferably in an automatic way, remains an important problem. While the automatic segmentation of high contrast structures like bones and lungs can be done in an acceptable period of time, a precise segmentation of structures such as vessels, liver or kidneys can currently not be performed automatically in a reliable manner within less than one to a few hours, as they are usually performed with manual or semi-automatic segmentation methods. This is a problem if the planning CT is acquired within minutes before the intervention. Waiting for those segmentation methods to improve in efficiency, we can propose to use incomplete but fully automatic segmentation to provide a rough automatic planning which can then be refined using interactive methods such as the proposed slice-based correction tool. Furthermore, we are currently investigating a new visualization scheme for interactively refining the trajectory based on a GPU based volume visualization restricted to the possible insertion zones. For this purpose, we virtually remove the skin around the insertion point and thus provide a view along the trajectory which allows determining the quality of the path..

In further investigations, cases of needle insertions without complications should be considered to examine whether the system is able to confirm valid entry points. In an ongoing clinical study, we are currently investigating the quality of the planning results and the usability of the planning system together with interventional radiologists with experience in RFA. First results were presented in this work and showed that the system is able to propose safe trajectories. However, in four cases the *umbrella constraint*, which takes into account the shape of the RFA needle, had to be disabled in order for the radiologists to find a satisfactory path. This may be attributed to the fact that only a rigid shape of the RFA umbrella is considered in the planning process, while in clinical routine the deployment of the umbrella's spikes may vary to avoid hitting critical structures. Consideration of the portal vein for computing the planning proposal would further improve the result of the planning. Because some proposed trajectories were rated safe and technically good but difficult to perform by the interventional radiologist due to the big insertion angle and trajectory length, the integration of the automatic trajectory planning in a navigation system such as proposed by Fichtinger *et al.* [28], Levy *et al.* [29] or Maier-Hein *et al.* [27] would be useful. These systems are potentially well-suited for transferring relatively long trajectories to the patient, thus allowing giving high weight to the *distance to critical structures constraint* to prevent complications. This integration would also reduce the procedure time for navigated needle interventions where the trajectory planning turned out to be the most time consuming part [27]. Future work will also include embedding the system into the clinical IT workflow of a PACS system (e.g. the Chili system [30]) to simplify the transfer and the processing of the medical imaging data.

In conclusion, the proposed trajectory planning approach clearly shows benefits compared to the current state-of-the-art planning in clinical routine. In contrast to the conventional planning, which is performed manually on the imaging data, our approach utilizes the three-dimensional information provided by the imaging modality in order to account for critical structures, angle of penetration, needle length, and needle shape. Thus, the system is able to quickly detect unsafe paths and propose safe trajectories during the planning which may especially be helpful for radiologists at the beginning or during their interventional training. We believe that our approach could improve the clinical procedure of needle insertions such as radiofrequency ablations or biopsies regarding complication rate and intervention time.

References

1 Pereira, P. L. Actual role of radiofrequency ablation of liver metastases. *Eur Radiol*, 17 (2007), 2062-2070.

2 Vaillant, Marc, Davatzikos, Christos, Taylor, Russell, and Bryan, R. A path-planning algorithm for image-guided neurosurgery. In *CVRMed-MRCAS'97* (1997), 467-476.

3 Brunenberg, Ellen J. L., Vilanova, Anna, Visser-Vanderwalle, Veerle, Temel, Yasin, Ackermans, Linda, Platel, Bram, and Romeny, Bart M ter Haar. Automatic trajectory planning for deep brain stimulation: a feasibility study. In *MICCAI* (Brisbane 2007), 584-592.

4 Shamir, Reuben R., Joskowicz, Leo, Antiga, Luca, Foroni, Roberto I., and Shoshan, Yigal. Trajectory planning method for reduced patient risk in image-guided neurosurgery: concept and preliminary results. In *SPIE Medical Imaging: Visualization, Image-Guided Procedures, and Modeling* (San Diego 2010), 76250I.

5 Shamir, Reuben R., Tamir, Idit, Dabool, Elad, Joskowicz, Leo, and Shoshan, Yigal. A method for

planning safe trajectories in image-guided keyhole neurosurgery. In *MICCAI* (Peking 2010), 457-464.

6 Navkar, Nikhil, Tsekos, Nikolaos, Stafford, Jason, Weinberg, Jeffrey, and Deng, Zhigang. Visualization and Planning of Neurosurgical Interventions with Straight Access. In *Information Processing in Computer-Assisted Interventions* (Geneva 2010), 1-11.

7 Essert, Caroline, Haegelen, Claire, and Jannin, Pierre. Automatic Computation of Electrodes Trajectory for Deep Brain Stimulation. *In proceedings of Medical Imaging and Augmented Reality (MIAR)*, LNCS 6326 (2010), 149-158.

8 Altrogge, Inga, Kröger, Tim, Preusser, Tobias et al. Towards optimization of probe placement for radio-frequency ablation. *Med Image Comput Comput Assist Interv*, 9 (2006), 486-493.

9 Weihusen, Andreas, Ritter, Felix, Pereira, Philippe L., Helmberger, Thomas, Hoffmann, Ralf-Thorsten, and Peitgen, Heinz-Otto. Towards a Workflow Oriented Software Assistance for the Radiofrequency Ablation. In *GI Jahrestagung* (2006), 507-513.

10 Butz, Torsten, War, Simon K., Tuncali, Kemal, Silverman, Stuart G., Sonnenberg, Eric Van, Jolesz, Ferenc A., and Kikinis, Ron. Pre- and intra-operative planning and simulation of percutaneous tumor ablation. In *Med Image Comput Comput Assist Interv* (Pittsburgh 2000), 317-326.

11 Zhai, Weiming, Xu, Jing, Zhao, Yannan, Song, Yixu, Sheng, Lin, and Jia, Peifa. Preoperative surgery planning for percutaneous hepatic microwave ablation. *Med Image Comput Comput Assist Interv*, 11 (2008), 569-577.

12 Villard, C., Soler, L., Papier, N., Agnus, V., Gangi, A., Mutter, D., and Marescaux, J. RF-Sim: a treatment planning tool for radiofrequency ablation of hepatic tumors. In *Proc. Seventh International Conference on Information Visualization* (London 2003), 561-567.

13 Villard, C., Soler, L., Gangi, A., Mutter, D., and Marescaux, J. Towards realistic radiofrequency ablation of hepatic tumors 3D simulation and planning. In *SPIE Medical Imaging* (San Diego 2004), Proceedings of SPIE, 586-595. Cum Laude poster award.

14 Villard, Caroline, Baegert, Claire, Schreck, Pascal, Soler, Luc, and Gangi, Afshin. Optimal trajectories computation within regions of interest for hepatic RFA planning. *Med Image Comput Comput Assist Interv*, 8 (2005), 49-56.

15 Baegert, Claire, Villard, Caroline, Schreck, Pascal, Soler, Luc, and Gangi, Afshin. Trajectory optimization for the planning of percutaneous radiofrequency ablation of hepatic tumors. *Comput Aided Surg*, 12 (2007), 82-90.

16 Baegert, Claire, Villard, Caroline, Schreck, Pascal, and Soler, Luc. Precise determination of regions of interest for hepatic RFA planning. *Stud Health Technol Inform*, 125 (2007), 31-36.

17 Baegert, Claire, Villard, Caroline, Schreck, Pascal, and Soler, Luc. Multi-criteria trajectory planning

for hepatic radiofrequency ablation. *Med Image Comput Comput Assist Interv*, 10 (2007), 676-684.

18 Schumann, Christian, Bieberstein, Jennifer, Trumm, Christoph et al. Fast automatic path proposal computation for hepatic needle placement. In *SPIE Medical Imaging* (San Diego 2010), SPIE, 76251J.

19 Wolf, Ivo, Vetter, Marcus, Wegner, Ingmar et al. The Medical Imaging Interaction Toolkit. *Med Image Anal*, 9 (2005), 594-604.

20 Maleike, Daniel, Nolden, Marco, Meinzer, Hans-Peter, and Wolf, Ivo. Interactive segmentation framework of the Medical Imaging Interaction Toolkit. *Comput Methods Programs Biomed*, 96 (2009), 72-83.

21 Mahnken, Andreas H. and Ricke, Jens. *CT- and MR-Guided Interventions in Radiology*. Springer, 2009.

22 Kirk, David. *Graphics Gems III*. Elsevier Science (USA), 1992.

23 Bentley, Jon Louis. Multidimensional binary search trees used for associative searching. *Commun. ACM* (1975), 509-517.

24 Stadler, W. A Survey of Multicriteria Optimization, or the Vector Maximum Problem. *J Optimiz Theory App*, 29 (1979), 1-52.

25 Stein, Daniel, Fritzsche, Klaus H., Nolden, Marco, and Meinzer, Hans-Peter. The extensible open-source rigid and affine image registration module of the Medical Imaging Interaction Toolkit (MITK). *Comput Methods Programs Biomed* (April 19, 2010).

26 Seppenwoolde, Yvette, Shirato, Hiroki, Kitamura, Kei, Shimizu, Shinichi, Herk, Marcel van, Lebesque, Joos V., and Miyasaka, Kazuo. Precise and real-time measurement of 3D tumor motion in lung due to breathing and heartbeat, measured during radiotherapy. *Int J Radiat Oncol Biol Phys*, 53 (2002), 822-34.

27 Maier-Hein, Lena, Tekbas, Aysun, Seitel, Alexander et al. In vivo accuracy assessment of a needle-based navigation system for CT-guided radiofrequency ablation of the liver. *Med Phys*, 35 (2008), 5386-5396.

28 Fichtinger, G., Deguet, A., Fischer, G. et al. Image overlay for CT-guided needle insertions. *Comp Aid Surg*, 10 (2005), 241-255.

29 Levy, E. B., Tang, J., Lindisch, D., Glossop, N., Banovac, F., and Cleary, K. Implementation of an electromagnetic tracking system for accurate intrahepatic puncture needle guidance: Accuracy results in an in vitro model. *Acad Radiol*, 14 (2007), 344-354.

30 Engelmann, Uwe, Schröter, Andre, U., Baur, Schwab, M., Werner, O., Makabe, M.H., and Meinzer, H.-P. Openness in (tele-) radiology workstations: The CHILI PlugIn concept. In *Computer Assisted Radiology and Surgery* (Tokyo 1998), 437-442.